CHINESE OPTICS LETTERS

Vol. 19, No. 4 | April 2021

Anisotropy of the thermal and laser output properties in Yb,Nd:Sc_2SiO_5 crystal

Yuqing Zhao (赵雨晴)[1], Qiangguo Wang (王强国)[1], Lihua Meng (孟丽华)[1], Yongping Yao (姚勇平)[1], Shande Liu (刘善德)[1,2*], Na Cui (崔 娜)[1], Liangbi Su (苏良碧)[3], Lihe Zheng (郑丽和)[4**], Huiyun Zhang (张会云)[1], and Yuping Zhang (张玉萍)[1***]

[1] College of Electronic and Information Engineering, Shandong University of Science and Technology, Qingdao 266590, China

[2] Collaborative Innovation Center of Light Manipulations and Applications, Shandong Normal University, Jinan 250358, China

[3] Key Laboratory of Transparent and Opto-functional Inorganic Materials, Artificial Crystal Research Center, Shanghai Institute of Ceramics, Chinese Academy of Sciences, Shanghai 200050, China

[4] School of Physics and Astronomy, Yunnan University, Kunming 650091, China

*Corresponding author: pepsl_liu@163.com

**Corresponding author: zhenglihe@ynu.edu.cn

***Corresponding author: sdust_thz@163.com

Received July 27, 2020 | Accepted October 19, 2020 | Posted Online February 5, 2021

The anisotropy of thermal property in an Yb,Nd:Sc_2SiO_5 crystal is investigated from the temperature of 293 to 573 K. Based on the systematical study of thermal expansion, thermal diffusivity, and specific heat, the thermal conductivity in Yb,Nd:Sc_2SiO_5 crystals orientated at (100), (010), (001), and (406) is calculated to be 3.46, 2.60, 3.35, and 3.68 $W/(m \cdot K)$, respectively. The laser output anisotropy of a continuous-wave (CW) and tunable laser is characterized, accordingly. A maximum output power of 6.09 W is achieved in the Yb,Nd:Sc_2SiO_5 crystal with (010) direction, corresponding to a slope efficiency of 48.56%. The tuning wavelength range in the Yb,Nd:Sc_2SiO_5 crystal orientated at (100), (010), and (001) is 68, 67, and 65 nm, separately. The effects of thermal properties on CW laser performance are discussed.

Keywords: anisotropy; thermal property; tunable laser; Yb,Nd:Sc_2SiO_5 crystal.

DOI: 10.3788/COL202119.041405

1. Introduction

Recently, studies on laser crystals have accelerated the developments of novel laser devices and technologies. Yb^{3+}-doped crystal lasers drew great attention in the 1 μm spectral region because of the quasi-three-level scheme of Yb^{3+} ions[1–3], which could effectively avoid occurrence of up-conversion, excited-state absorption, concentration quenching, and cross relaxation. Besides, low quantum defects could increase laser efficiency and reduce generation of thermal effects. In particular, the broad absorption and emission bands of the Yb^{3+}-doped crystals make it suitable for ultrafast and tunable laser operations. Many researchers make great efforts on Yb-doped gain medium and obtain lots of encouraging achievements. A 25.6 MW, high peak power Yb:$Y_3Al_5O_{12}$ (Yb:YAG) femtosecond laser was reported by Saraceno *et al.*[4]. In 2017, Toci *et al.* reported growth of a Yb:$Gd_3Al_2Ga_3O_{12}$ (Yb:GAGG) crystal, spectral properties, and laser output characteristics[5]. Nevertheless, the main defect of the Yb^{3+}-doped crystal is that the laser threshold is relatively high. The large crystal field strength in oxy-orthosilicate crystals could increase the manifold splitting of energy states in Yb^{3+} ions, which could partly overcome the shortage of high pump power threshold[6]. Due to the unique property of negative thermo-optical coefficient dn/dT, the Sc_2SiO_5 crystal is regarded as a promising laser crystal for ultrafast and high-power laser applications[7–9]. The mode-locked Yb:Sc_2SiO_5 laser with a pulse width of 2.3 ps was first reported by Li *et al.*[10]. Wentsch *et al.* reported an Yb:Sc_2SiO_5 thin-disk laser with a output power of 9.4 W in 2012[11]. However, the low emission cross section of the Yb:Sc_2SiO_5 crystal limits the power extraction. Benefiting from energy transfer between Nd^{3+} ions and Yb^{3+} ions, an $(Yb_{0.05}Nd_{0.03}Sc_{0.947})_2SiO_5$ (Yb,Nd:Sc_2SiO_5) single crystal was grown in order to augment the gain cross section of the Yb:Sc_2SiO_5 crystal. Compared with the Yb:Sc_2SiO_5 crystal, the emission cross section of the Yb,Nd:Sc_2SiO_5 crystal increases by 18.9%[12]. A 3 W continuous-wave (CW) laser and a ultrafast laser with pulse width of 367 fs were achieved in a *b*-cut Yb,Nd:Sc_2SiO_5 crystal[13]. It is noticed that the Yb,Nd:Sc_2SiO_5 crystal possesses anisotropy properties due to the characterization of the monoclinic crystal

structure. It is of significance in understanding the anisotropy of thermal and laser properties to design Yb,Nd:Sc_2SiO_5 laser devices.

In this Letter, thermal anisotropy in the Yb,Nd:Sc_2SiO_5 crystal was investigated. The thermal properties including thermal expansion, thermal diffusivity, and specific heat of the Yb,Nd:Sc_2SiO_5 crystal were systematically studied from the temperature of 293 to 573 K. The thermal conductivity was determined accordingly. The CW and tuning characteristics of the Yb,Nd:Sc_2SiO_5 crystal lasers along different principal directions were investigated.

2. Experimental Setup

The buoyancy method was used to measure density of the Yb,Nd:Sc_2SiO_5 crystal at room temperature. The whole process is carried out without the crystal touching the bottom of the beaker. Specific heat of the Yb,Nd:Sc_2SiO_5 crystal was measured by using a differential scanning calorimeter (DSC, Perkin-Elmer Diamond model DSC-ZC). A laser pulse method was applied to measure thermal diffusion coefficient of the Yb,Nd:Sc_2SiO_5 crystal (apparatus: Netzsch Nano-flash model LFA 447). A thermal–mechanical analyzer (Diamond TMA, Perkin-Elmer Co.) was employed to measure thermal expansion coefficient of the Yb,Nd:Sc_2SiO_5 crystal. The measuring temperature range was from 299 to 772 K with a heating step of 5 K/min.

Figure 1 shows a schematic of the laser experiments. A 976 nm laser diode was selected as a pump source with a maximum pump power of 30 W. The pump light was delivered into the Yb,Nd:Sc_2SiO_5 crystal with an imaging system. The pump waist in the Yb,Nd:Sc_2SiO_5 crystal was about 200 μm. The uncoated Yb,Nd:Sc_2SiO_5 crystals cut along the principal axis (X, Y, and Z) were employed as laser medium. All of the laser crystals were wrapped by indium and mounted in a copper block in order to efficiently reduce the influence of the thermal effect. The cooling temperature for the copper block was maintained at 16°C. Mirrors M_1, M_3, and M_4 were all processed with antireflection (AR) coating around 976 nm and high-reflection coating (HR, $R > 99.9\%$) at 1030–1100 nm. The mirror radii of curvature were $r = 200$, $r = \infty$, and $r = 200$ mm, respectively. The output mirrors M_2 and M_5 were both partial transmittance ($T_{oc} = 1\%$, 3%, 10%, and 25%) coated at 1030–1100 nm. As shown in Fig. 1(b), a quartz birefringent filter (BF) was employed in the tunable laser experiment to achieve laser tuning operation. The size of the BF was $\Phi 25 \times 3$ mm. A laser power meter (Fieldmax-II, Coherent) was employed to measure laser power. The laser output spectra were measured by a spectrometer (Avantes, AcaSpec-3468-NIR256-2.2).

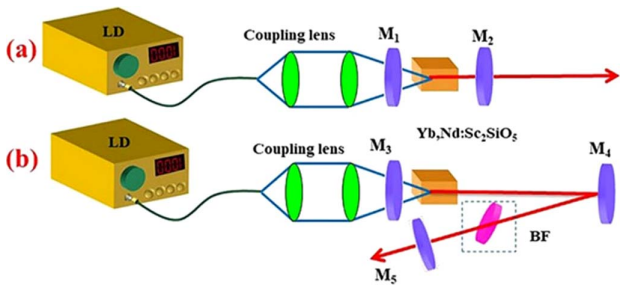

Fig. 1. Experimental setup of Yb,Nd:Sc_2SiO_5 lasers. (a) CW laser; (b) tunable laser.

3. Results and Discussion

The thermal expansion coefficient tensor of the monoclinic Yb,Nd:Sc_2SiO_5 crystal in the conventional orientation can be expressed by Eq. (1):

$$\begin{pmatrix} \alpha_{11} & 0 & \alpha_{13} \\ 0 & \alpha_{22} & 0 \\ \alpha_{31} & 0 & \alpha_{33} \end{pmatrix}. \tag{1}$$

As can be seen, α_{11}, $\alpha_{31}(=\alpha_{13})$, α_{22}, and α_{33} are four independent thermal components. Therefore, thermal expansion coefficients of four different crystal orientations are required to determine α_{ij}. In our experiment, four Yb,Nd:Sc_2SiO_5 crystal samples cut along (100), (010), (001), and (406) orientations are prepared. By calculation, the four independent principal thermal components in Eq. (1) could be diagonalized in Eq. (2):

$$\begin{pmatrix} 1.781 & 0 & 0 \\ 0 & 11.864 & 0 \\ 0 & 0 & 16.137 \end{pmatrix}. \tag{2}$$

Density of the Yb,Nd:Sc_2SiO_5 crystal could be calculated by Eq. (3):

$$\rho = \frac{\rho_0}{\left(1+\frac{\Delta a}{a_0}\right)\left(1+\frac{\Delta b}{b_0}\right)\left(1+\frac{\Delta c}{c_0}\right)}. \tag{3}$$

Here, ρ_0 is density at room temperature. $\Delta a/a_0$, $\Delta b/b_0$, and $\Delta c/c_0$ denote the thermal expansion coefficients of the Yb,Nd:Sc_2SiO_5 crystal along crystallographic axes of (100), (010), and (001), respectively. Thermal conductivity k of the Yb,Nd:Sc_2SiO_5 crystal was calculated through Eq. (4), where λ, C_p, and ρ denote the thermal diffusion coefficient, specific heat, and density of the Yb,Nd:Sc_2SiO_5 crystal, respectively:

$$k = \lambda \rho C_p. \tag{4}$$

Figure 2(a) shows the relationship between specific heat and temperature. The specific heat is enhanced linearly from 0.641 to 0.999 $J \cdot g^{-1} \cdot K^{-1}$ with temperature increasing from 293 to 573 K. The experimental data presents that the Yb,Nd:Sc_2SiO_5 crystal possesses the advantage of tolerating more thermal energy. Figure 2(b) displays thermal diffusion coefficients of the Yb,Nd:Sc_2SiO_5 crystal along the (100), (010), (001), and (406) directions at the temperatures ranging from 299 to 522 K. The achieved thermal diffusion coefficients were 1.486, 1.359, 1.336, and 1.553 mm^2/s in Yb,Nd:Sc_2SiO_5 crystals along crystallographic axes of (100), (010), (001), and (406) at room temperature. Figure 2(c) displays the thermal expansion

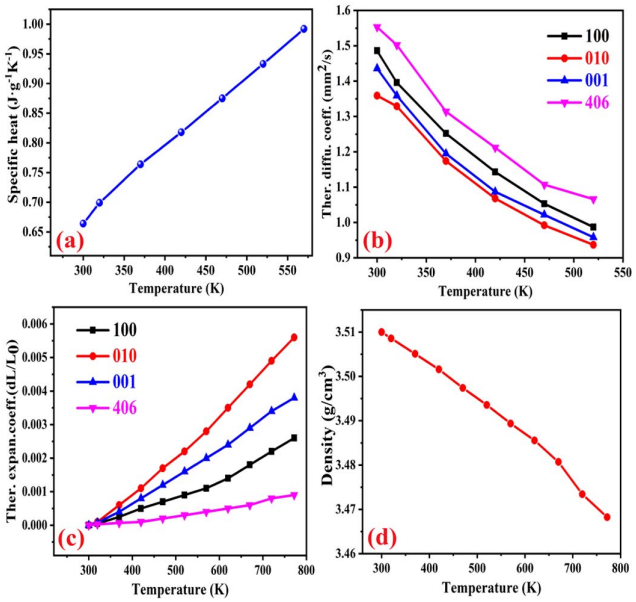

Fig. 2. Thermal properties of the Yb,Nd:Sc_2SiO_5 crystal versus temperature. (a) Specific heat; (b) thermal diffusion coefficient; (c) thermal expansion coefficient; (d) density.

coefficient as a function of temperature. It can be observed that the thermal expansion coefficient variation is almost linear over the entire temperature range. Figure 2(d) presents density values at different temperatures. Density of the Yb,Nd:Sc_2SiO_5 crystal is 3.51 g · cm^{-3} at room temperature.

Figure 3 depicts the relationship between the thermal conductivity and temperature. Thermal conductivity of the Yb,Nd:Sc_2SiO_5 crystal decreases with the increasing temperature.

Thermal conductivity of the Yb,Nd:Sc_2SiO_5 crystal at room temperature is 3.46, 2.60, 3.35, and 3.68 W/(m·K) along the (100), (010), (001), and (406) axes, respectively.

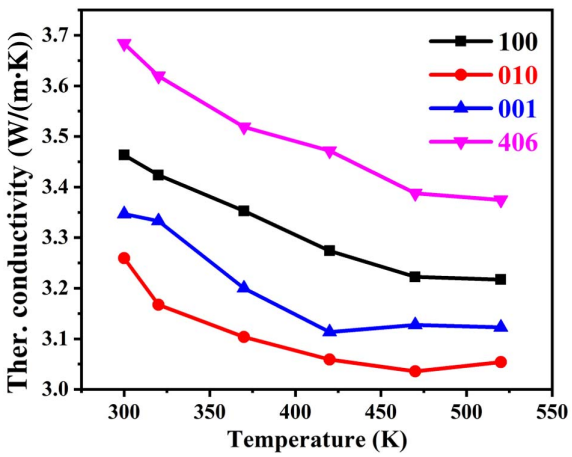

Fig. 3. Calculated thermal conductivity in a single Yb,Nd:Sc_2SiO_5 crystal.

The monoclinic structure of the Yb,Nd:Sc_2SiO_5 crystal belongs to the crystal system of $C_{2/c}$, which indicates an anisotropy performance of the laser output property. Thus, the orientation of the principal axis was determined. The angles between crystallographic axes (*a*, *b*, *c*) in the Yb,Nd:Sc_2SiO_5 crystal are $\beta_{ab} = \beta_{bc} = 90°$ and $\beta_{ac} = 103.8°$. In the monoclinic structure of the Yb,Nd:Sc_2SiO_5 crystal, crystallographic axis *b* is one of the principal axes that are collinear with the two-fold axis. The other two principal axes locating in the (010) face are at an angle to the crystallographic axes *a* and *c*, respectively. A *b*-cut Yb,Nd:Sc_2SiO_5 crystal sample with thickness of 1 mm was measured by an XPT-6-type polarized microscope to determine the angle relationship. Figure 4 shows the relationship between the principal axis and the crystallographic axis. The (010) face is perpendicular to the crystallographic axis *b*. The angle between crystallographic axis *a* and principal axis *Z* is measured to be 21.2°. Besides, that between crystallographic axis *c* and principal axis *Y* is 35°.

A linear laser cavity is designed to investigate anisotropy of the CW laser output properties of the Yb,Nd:Sc_2SiO_5 crystals. The CW output power versus absorbed pump power is shown in Fig. 5. As can be seen, the effect of anisotropy on laser output power was observed obviously. The maximum average output power of 6.09 W is generated in the *X*-cut Yb,Nd:Sc_2SiO_5 crystal, corresponding to a slope efficiency of 48.56%. The anisotropy of laser output power may be partly attributed to the anisotropy of thermal properties. The expansion coefficients and thermal conductivities along the *a* axis and *c* axis are similar to and higher than that of the *b* axis. In our experiment, the maximum absorbed pump power is 15.3 W in the (*b* axis) *X*-cut Yb,Nd:Sc_2SiO_5 crystal, which is higher than that of the *Y*-cut and *Z*-cut Yb,Nd:Sc_2SiO_5 crystals. It clarifies that the *X*-cut Yb,Nd:Sc_2SiO_5 crystal possesses relatively uniform thermal expansion and better heat dissipation along the radial

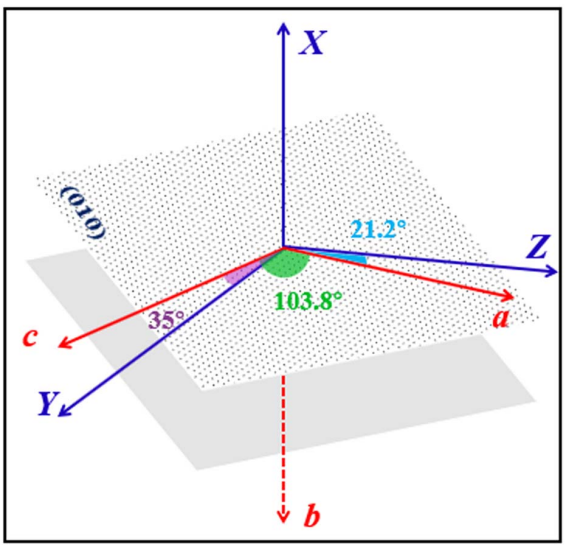

Fig. 4. Relationship between the principal axis and crystallographic axis (*a*, *b*, *c*) in the Yb,Nd:Sc_2SiO_5 crystal.

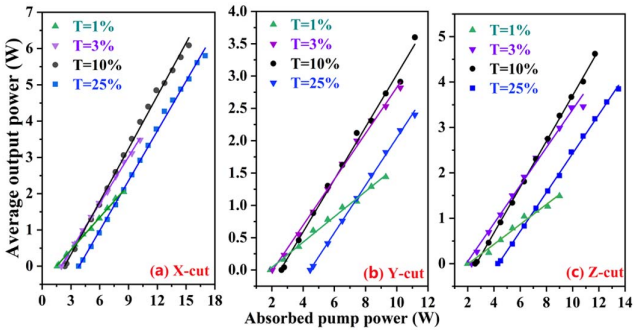

Fig. 5. Average output power versus absorbed pump power along different principal axes in the Yb,Nd:Sc_2SiO_5 crystal.

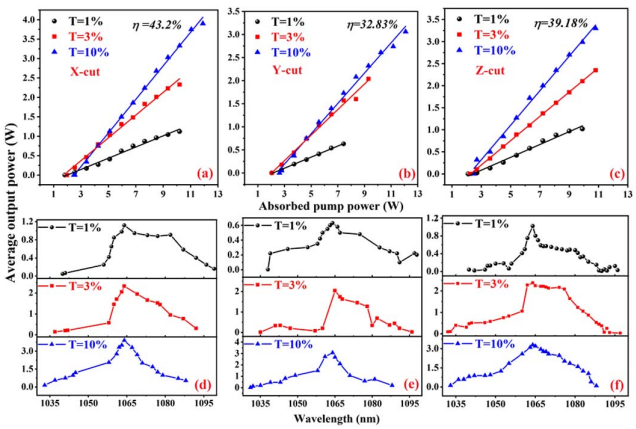

Fig. 6. Tunable characteristics of the Yb,Nd:Sc_2SiO_5 crystals. (a), (d) *X*-cut crystal; (b), (e) *Y*-cut crystal; (c), (f) *Z*-cut crystal.

direction. Meanwhile, it is worth noting that Fresnel reflection loss in the uncoated Yb,Nd:Sc_2SiO_5 crystal is above 10%, which increases the lasing threshold and limits the output power.

As shown in Fig. 1(b), a BF was inserted into the laser cavity at a Brewster angle to achieve laser tuning. Figures 6(a)–6(c) depict the relationship between output power and absorbed pump power with the V-type cavity. Compared with the linear cavity, output power achieved with V-type cavity was relatively lower because of the polarization and insertion loss. Under an absorbed pump power of 11.9 W, the maximum average output power of 3.9 W was obtained with the *X*-cut Yb,Nd:Sc_2SiO_5 crystal, corresponding to a slope efficiency of 43.2%. Laser polarization was measured by guiding the laser beam passing through a half-waveplate and a polarizing beam splitter (PBS). The polarization is parallel to the *Y* direction of the *X*-cut crystal, to *Z* direction of the *Y*-cut crystal, and to *X* direction of the *Z*-cut crystal. The laser wavelength could be flexibly tuned

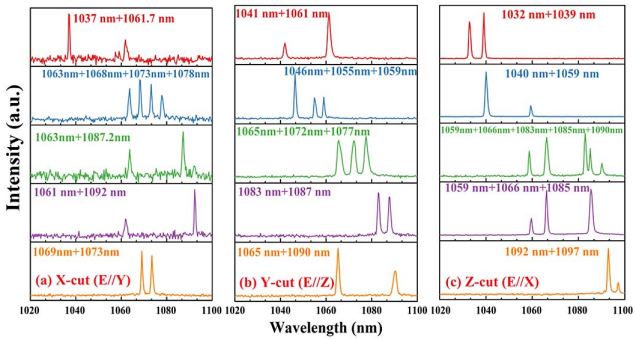

Fig. 7. Multi-wavelength laser output spectra. (a) *X*-cut crystal; (b) *Y*-cut crystal; (c) *Z*-cut crystal.

Table 1. Anisotropy of Output Parameters in an Yb,Nd:Sc_2SiO_5 Crystal Laser.

		CW		Tunable			
Crystal Orientation	T_{oc} (%)	P_{max} (W)	η (%)	P_{thr} (W)	P_{max} (W)	η (%)	Tuning Coverage (nm)
X-cut ($E\|\|Y$)	1	2.05	29.78	1.82	0.12	14.42	1040–1099 (59)
	3	3.48	42.80	1.97	2.33	29.27	1037–1092 (55)
	10	6.09	48.56	2.49	3.90	43.20	1031–1088 (57)
Y-cut ($E\|\|Z$)	1	1.44	19.60	2.05	0.63	11.98	1038–1098 (60)
	3	2.82	35.52	2.06	2.04	27.64	1035–1096 (61)
	10	3.60	40.56	2.62	3.06	32.83	1031–1088 (57)
Z-cut ($E\|\|Z$)	1	1.49	21.96	2.10	1.02	14.57	1040–1096 (56)
	3	3.46	41.81	2.23	2.35	27.59	1032–1097 (65)
	10	4.62	50.43	2.50	3.30	39.18	1033–1088 (55)

Note: T_{oc}, output coupler transmittance; P_{thr}, pump threshold; P_{max}, maximum output power; η, slope efficiency.

in the emission band by carefully varying the BF. Figures 6(d)–6(f) present the tuning wavelength versus the corresponding output power at different transmittances. The CW tuning coverage is 68, 67, and 65 nm in *X*-, *Y*-, and *Z*-cut Yb,Nd:Sc_2SiO_5 crystals, corresponding to tuning ranges of 1031–1099, 1031–1098, and 1032–1097 nm, respectively. The CW and tunable laser parameters including laser threshold, output power, and tuning coverage of Yb,Nd:Sc_2SiO_5 are listed in Table 1. The multi-wavelength laser is achieved by adjusting the insertion angle of the BF. The emergence of gain competition between various wavelengths led to the occurrence of simultaneous multi-wavelength oscillation. Figures 7(a)–7(c) record the multi-wavelength spectra of the Yb,Nd:Sc_2SiO_5 crystal with $T_{oc} = 1\%$.

4. Conclusions

In conclusion, the anisotropy of the thermal and laser output properties in the Yb,Nd:Sc_2SiO_5 crystal was fully studied. The room temperature thermal conductivity is 3.46, 2.60, 3.35, and 3.68 W/(m· K) along crystallographic axes of (100), (010), (001), and (406), respectively. Due to relatively uniform thermal expansion along the radial direction and better heat conduction along the *X* direction of the Yb,Nd:Sc_2SiO_5 crystal, the maximum output power of 6.09 W was generated in the *X*-cut Yb,Nd:Sc_2SiO_5 crystal. The tuning ranges of the Yb,Nd:Sc_2SiO_5 tunable laser are 68 nm, 67 nm, and 65 nm for *X*-, *Y*-, and *Z*-cut crystals, respectively.

Acknowledgement

This work was supported by the Natural Science Foundation of Shandong Province (No. ZR2020MF115), the National Key Research and Development Program of China (No. 2017YFA0701000), the National Natural Science Foundation of China (Nos. 61875106, 61775123, and U1830104), the Key Research and Development Program of Shandong Province (Nos. 2019GGX104039 and 2019GGX104053), and the SDUST Research Fund (No. 2019TDJH103).

References

1. W. L. Tian, Y. N. Peng, Z. Y. Zhang, Z. J. Yu, J. F. Zhu, X. D. Xu, and Z. Y. Wei, "Diode-power scalable Kerr-lens mode-locked Yb:CYA laser," Photon. Res. **6**, 127 (2018).
2. M. Zhao, C. Wang, Q. Hao, Z. Zou, J. Liu, X. Fan, and L. Su, "High single-pulse energy passively *Q*-switched laser based on Yb,Gd:SrF_2 crystal," Chin. Opt. Lett. **18**, 101401 (2020).
3. G. Qian, H. L. Zhang, and J. Fayyaz, "Laser diode partially end-pumped electro-optically *Q*-switched Yb:YAG slab laser," Chin. Opt. Lett. **17**, 111405 (2019).
4. C. J. Saraceno, F. Emaury, O. H. Heckl, C. R. E. Baer, M. Hoffmann, C. Schriber, M. Golling, T. Südmeyer, and U. Keller, "275 W average output power from a femtosecond thin disk oscillator operated in a vacuum environment," Opt. Express **20**, 23535 (2012).
5. G. Toci, A. Pirri, W. Ryba-Romanowski, M. Berkowski, and M. Vannini, "Spectroscopy and CW first laser operation of Yb-doped $Gd_3(Al_{0.5}Ga_{0.5})_5O_{12}$ crystal," Opt. Mater. Express **7**, 170 (2017).
6. P. H. Haumesser, R. Gaumé, B. Viana, E. Antic-Fidancev, and D. Vivien, "Spectroscopic and crystal-field analysis of new Yb-doped laser materials," J. Phys.: Condensed Matter. **13**, 5427 (2001).
7. L. Zheng, J. Xu, G. Zhao, L. Su, F. Wu, and X. Liang, "Bulk crystal growth and efficient diode-pumped laser performance of Yb^{3+}:Sc_2SiO_5," Appl. Phys. B **91**, 443 (2008).
8. H. Y. Zhang, J. F. Li, X. Y. Liang, H. Lin, L. H. Zheng, L. B. Su, and J. Xu, "High-power and wavelength tunable diode-pumped continuous wave Yb:SSO laser," Chin. Opt. Lett. **10**, 111404 (2012).
9. W. D. Tan, D. Y. Tang, X. D. Xu, J. Zhang, C. W. Xu, F. Xu, L. H. Zheng, L. B. Su, and J. Xu, "Passive femtosecond mode-locking and cw laser performance of Yb^{3+}:Sc_2SiO_5," Opt. Express **18**, 16739 (2010).
10. J. F. Li, X. Y. Liang, J. P. He, L. H. Zheng, Z. W. Zhao, and J. Xu, "Diode pumped passively mode-locked Yb:SSO laser with 2.3 ps duration," Opt. Express **18**, 18354 (2010).
11. K. S. Wentsch, B. Weichelt, L. H. Zheng, J. Xu, M. A. Ahmed, and T. Graf, "Continuous-wave Yb-doped Sc_2SiO_5 thin-disk laser," Opt. Lett. **37**, 4750 (2012).
12. Z. G. Zou, L. H. Zheng, J. T. Wang, D. P. Jiang, S. D. Liu, Q. L. Sai, J. Y. Wang, H. Hu, and L. B. Su, "Crystal growth and photoluminescence spectra properties of $(Yb_xNd_ySc_{1-x-y})_2SiO_5$ laser crystal," Laser Phys. Lett. **15**, 085703 (2018).
13. L. L. Dong, Y. P. Yao, Q. G. Wang, S. D. Liu, L. H. Zheng, Y. Xu, D. H. Li, H. H. Zhang, Z. Y. Zou, and L. B. Su, "Tunable and mode-locking Yb,Nd:Sc_2SiO_5 femtosecond laser," IEEE Photon. Technol. Lett. **30**, 2167 (2018).